JMEPEG
https://doi.org/10.1007/s11665-024-09204-0

1059-9495/$19.00

ORIGINAL RESEARCH ARTICLE

Investigation of Grain Refinement and Mechanical Properties of Al-7Si Alloy with Al-5Nb-1B Master Alloy Addition Treated by Ultrasound Treatment

Kailong Wang, Qinglin Li, Jie Zhang, and Ziqi Zhang

Submitted: 31 August 2023 / Revised: 13 December 2023 / Accepted: 1 January 2024

In this research, a novel Al-5Nb-1B master alloy refiner was prepared based on traditional casting methods with the aid of ultrasonic melt-assisted treatment. The outcomes showed that as the ultrasonic power was increased, the primary α-Al and precipitates in Al-5Nb-1B alloy were greatly refined. Among them, the coarse cellular α-Al structure was transformed into fine equiaxed grains, and their size was significantly decreased from 125 to 60 μm when the melt was treated by 1500 W ultrasound power. In addition, the size and shape of Al_3Nb and NbB_2 phases were optimized after 1000 W ultrasound treatment, and the agglomeration of particles was also effectively eliminated. Meanwhile, the nano-sized NbB_2 particles precipitated from Al-5Nb-1B alloy after ultrasonic melt treatment. The influences of acoustic cavitation and acoustic streaming on the characterization of the microstructure in Al-5Nb-1B alloy were analyzed. Subsequently, the α-Al phase was greatly refined into fine equiaxed grains when Al-5Nb-1B master alloy treated by 1000 W ultrasonic power was added to Al-7Si alloy. Moreover, the secondary dendrites arm spacing was significantly decreased to 9.78 μm. Additionally, the tensile testing revealed that the ultimate tensile strength of Al-7Si alloy with the addition of Al-5Nb-1B master alloy was enhanced by 7.1% from 171 to 188.5 MPa, and the elongation was improved by 74.6% from 7.1 to 11.8%.

Keywords Al-5Nb-1B alloy, Al-7Si alloy, grain refinement, mechanical properties, ultrasound treatment

1. Introduction

It has been proved that the grains refinement is one of the most efficient ways to improve casting quality through increasing melt fluidity and reducing casting defects including internal shrinkage, porosity, segregation, and hot cracking (Ref 1). Owing to the superior refining efficiency and low cost, Al-5Ti-1B refiner is commonly employed in the refining pure aluminum and wrought aluminum alloys (Ref 2). However, Al-5Ti-1B alloy has a few disadvantages. When the Si concentration surpasses 4 wt.% in cast aluminum alloys, the Ti element reacts with Si in the Al-Si alloys melt and forms binary or ternary silicides, such as $TiSi_2$, $AlSi_3Ti_2$, or $(Al, Si)_3Ti$ (Ref 3, 4). The effect of grains refining significantly decreases due to the precipitation of silicides, resulting in the reduction of TiB_2 and Al_3Ti particles acting as heterogeneous nuclei (Ref 5). The phenomenon is known as the poisoning effect of refiner (Ref 5-7). Recently, some researchers have proposed the utilization of novelty Al-B master alloy (Ref 8), Al-Ti-B-C master alloy (Ref 9), and Al-Nb-B refiners to solve this problem.

Nowak et al. (Ref 10) originally developed Al-Nb-B alloys and concluded that Al-Nb-B alloys as grain refiners of hypoeutectic and eutectic Al-Si alloys can effectively refine the dendritic α-Al and do not encounter obviously poisoning effect. This is due to the fact that the Nb-Si binary phase is more stable at high temperatures than the Ti-Si binary phase (Ref 11, 12). Bolzoni et al. (Ref 13, 14) discovered that the addition of Al-Nb-B grain refiners into LM6 and LM25 aluminum alloys can not only refine significantly the microstructure of the alloys but also reduce the dependency of grain size variation in solidification (i.e., cooling rate). Xu et al. (Ref 15) optimized the composition of Al-Nb-B refiner based on the design criteria of Al_3Nb phase fraction and NbB_2 number density and found that the optimized refiner can decrease the grain size of Al-9Si-0.08Ti alloy and Al-10Si alloy less than 220 μm.

However, the nucleation particles of NbB_2 and Al_3Nb in Al-Nb-B alloys easily agglomerate, which lead to a reduction of refining efficiency. Recently, it has been found in previous literature (Ref 16, 17) that UT can enhance the wettability between reinforcement materials and metal matrix. Jung et al. (Ref 18) demonstrated that the grain size of α-Al phases, Si phases, and the precipitates in Al-Si piston alloys were effectively refined with the aid of ultrasonic melt treatment, which was attributed to enhancing nucleation of the phases during solidification. Liu et al. (Ref 19) concluded that when UT was used in the preparation of Al-4.5Cu composites with nano-TiB_2 particle reinforcement, the ultimate tensile strength (UTS) showed a promising improvement of 4.5%, rising from 196 to 205 MPa, and the elongation (El) was improved by

Kailong Wang, Qinglin Li, Jie Zhang, and **Ziqi Zhang**, School of Materials Science and Engineering, Lanzhou University of Technology, Lanzhou 730050, China; and State Key Laboratory of Advanced Processing and Recycling of Nonferrous Metals, Lanzhou University of Technology, Lanzhou 730050, China. Contact e-mail: liql301@mail.nwpu.edu.cn.

Published online: 08 February 2024

3.3% from 13.65 to 14.10%. Han et al. (Ref 20) used ultrasound assistance in the fabrication of Al-Ti-B grain refiners and concluded that the $TiAl_3$ particles were transferred into a short rod and the aggregated TiB_2 particles were transformed into a loose coral-like structure. Wu et al. (Ref 21) found that the ultrasonic treatment can reduce solute segregation of Mg-5Sm-Al alloy, and refine the grains of as-cast alloy in solidification.

Based on the above literature reports, with the aim to decrease the size of NbB_2 and Al_3Nb particles and make the uniformity of particle distribution, and improve the refinement effect of Al-7Si alloy, a novel Al-5Nb-1B grain refiners was prepared by ultrasonic melt-assisted treatment. The work investigated the impact of different ultrasonic powers on the microstructure evolution in the Al-5Nb-1B grain refiners, including the changes of the primary α-Al phase, as well as the morphology, size, and distribution state of Al_3Nb and NbB_2 precipitates. Furthermore, the effect of the addition of Al-5Nb-1B master alloy on the microstructure and mechanical properties of Al-7Si alloy was also discussed.

2. Experimental

2.1 The Process of Preparing Al-5Nb-1B Alloy

The Al-5Nb-1B master alloy was fabricated employing industrial pure aluminum (99.7% purity), Al-10Nb alloy, and Al-3B alloy as raw materials. The elemental composition of the different materials is shown in Table 1.

Al-10Nb alloy and Al-3B alloy were placed in a drying oven at 300 °C to remove moisture. In a graphite clay crucible, pure aluminum ingots were melted by an electrical resistance furnace. Al-Nb-B alloy containing an Nb/B ratio of 5:1 was fabricated by adding Al-10Nb and Al-3B to the Al melt at 850 °C and holding for 2 h. After the removal of the reaction slag, the UT was fulfilled at the temperature of 760 °C, and the amplitude change rod was inserted into the melt below the surface at 1 cm through a Ti-6Al-4V alloy radiator with a diameter of 2.4 cm. In the UT process, the ultrasonic generator was operated at a fixed frequency of 20 kHz, while the ultrasonic power was set to 500, 1000, and 1500 W, respectively. After 3 min UT, the melt temperature of the Al-5Nb-1B alloy was gradually cooled to 680 °C and then poured into a preheated permanent steel mold. In addition, the samples of Al-5Nb-1B master alloy prepared under different powers were named S1, S2, S3, and S4, respectively.

2.2 Preparation of Refined Al-7Si Alloys

The hypoeutectic Al-7Si alloy utilized in this investigation was made from commercial hypereutectic Al-20Si alloy and pure Al. Firstly, the master alloy prepared at 0, 500, 1000, and 1500 W is placed in a drying furnace to remove moisture. Then, the Al-7Si alloy was placed in a clay-bonded graphite crucible and held at 800 °C for 2 h. The samples of S0, S1, S2, S3, and S4 were added to the Al-7Si alloy with a target addition amount of 0.1 wt.%Nb and kept at the temperature for 60 minutes. When the melt temperature reached 720 °C, the hexachloroethane (C_2Cl_6) was added to melt to remove gas and slag. Finally, the Al-7Si alloy melting was poured into a preheated mold.

2.3 Characterization

The samples were obtained at the same height from each ingot, then grinded and polished before being etched with 4% nitric acid alcohol. To identify the phase component of Al-5Nb-1B alloy, x-ray diffraction (XRD, D/max-2400) was used with Cu Kα radiation. The mapping distribution of elements in Al-5Nb-1B alloy was fulfilled by EPMA1600. To examine the microstructural characterization of the samples, scanning electron microscopy (SEM, FEG-450) combined with an energy-dispersive spectrometer (EDS) was employed during the analysis. The size of the particles and the secondary dendrites arm spacing (SDAS) of α-Al were measured using image software. According to the GB/T228.1-2021 standard, three tensile test samples were carefully selected to evaluate the mechanical properties. The tests were performed by a materials testing machine (AGS-X 300 KN, Shimadzu) at a speed of 1.0 mm/min. SEM was additionally employed to examine the fracture surfaces of the samples.

3. Results and Discussions

3.1 The Evolution of a-Al

Figure 1 and 2 show the morphology evolution and the change of average grain size of α-Al in S1, S2, S3, and S4 alloys, respectively. Figure 1a illustrates the morphology of α-Al in the untreated Al-5Nb-1B alloy. The micrograph clearly reveals that the α-Al grains are coarse cellular crystals with a mean size of 125 μm. It can be found from S2 alloy that the shape of the α-Al happens to obviously change from cellular crystals to equiaxed crystals (Fig. 1b). At the same time, the grain size is also significantly reduced. In S3 alloy, as shown in Fig. 1(c), the mean grain size decreases to 71 μm, and the proportion of equiaxed crystals is significantly increased. In addition, the primary α-Al of S4 alloy is entirely transformed into fine equiaxed crystals and the average size reduces to 60 μm, as shown in Fig. 1(d). The results demonstrate that the refining effect of α-Al grains in Al-5Nb-1B alloy can be influenced by UT power. Moreover, the higher the ultrasound

Table 1 Elemental composition (wt.%) of the different materials

	Element concentration, wt.%							
Alloys	**Nb**	**B**	**Si**	**Cu**	**Ti**	**Fe**	**Ni**	**Al**
Al-10Nb	9.98	…	0.035	…	…	0.082	< 0.01	Bal
Al-3B	…	3.01	0.11	…	…	0.19	…	Bal
CP-Al	…	…	< 0.003	< 0.005	< 0.05	< 0.03	…	Bal

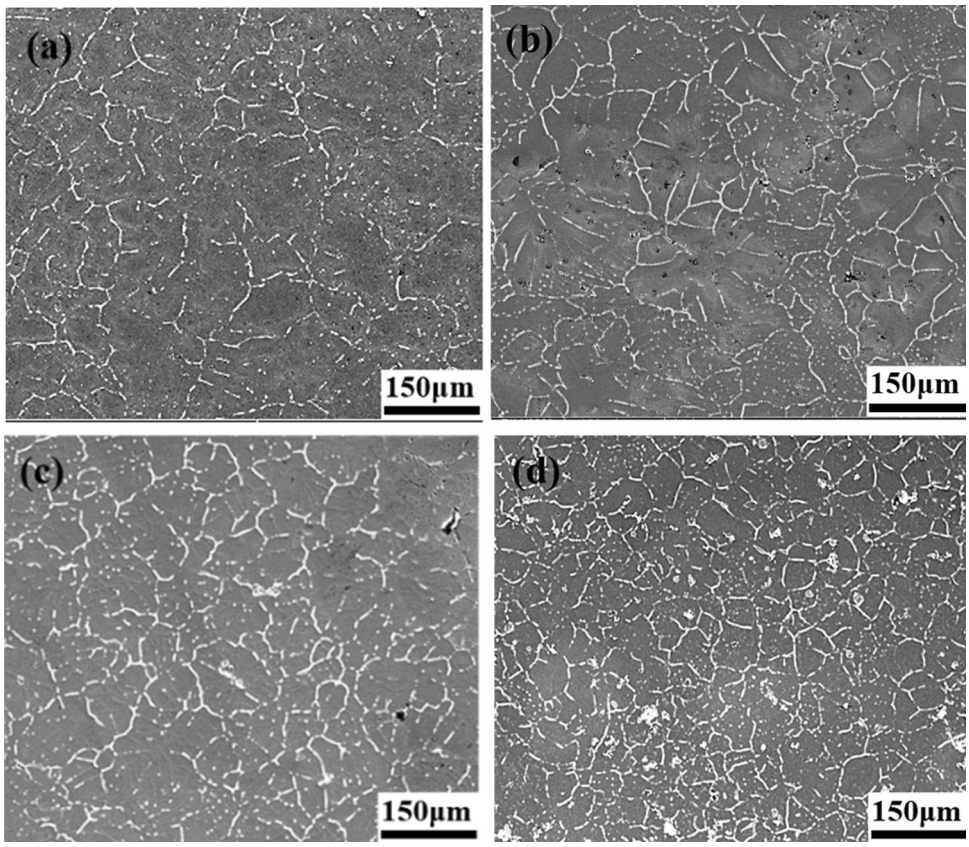

Fig. 1 SEM images of α-Al in Al-5Nb-1B alloy under different ultrasonic power conditions: (a) S1; (b) S2; (c) S3; (d) S4

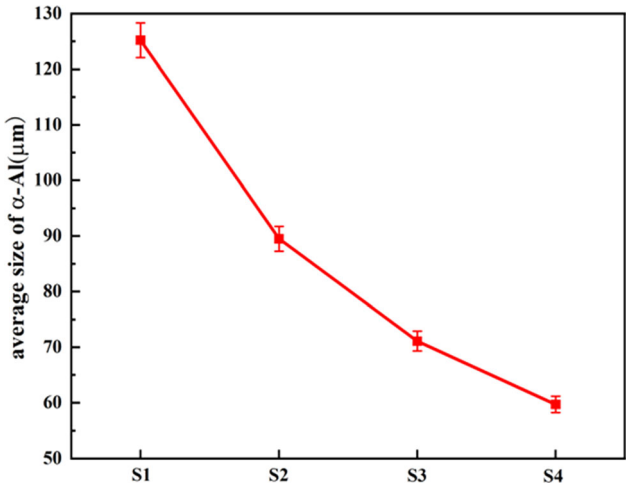

Fig. 2 Effect of ultrasonic power on the average size of α-Al in Al-5Nb-1B alloy

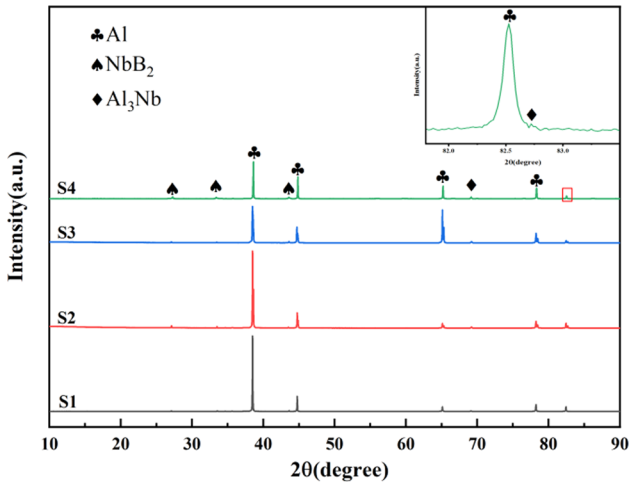

Fig. 3 XRD patterns of Al-5Nb-1B alloy prepared with different ultrasonic power conditions

power, the smaller the grains size of α-Al is in Al-5Nb-1B alloy with UT.

3.2 The Evolution of Precipitates

Figure 3 indicates the XRD patterns of Al-5Nb-1B alloy melting treated by different ultrasonic power. It can be obviously observed that α-Al, NbB_2, and Al_3Nb phases are detected in all four alloy samples. The result shows that the UT applied in Al-5Nb-1B alloy melt does not alter the phase constituent. Figure 4 depicts the composition analysis of the particle precipitation from the Al-5Nb-1B alloy treated by 1000 W ultrasonic vibration. It can be observed from Fig. 4 that the two kinds of particles with different morphology distribute within primary α-Al matrix in Al-5Nb-1B alloy: a white block/segregation phase (showed by the red circle in Fig. 4a) and a gray block phase (indicated by the yellow square in Fig. 4a). In Fig. 5, the EPMA mapping analysis of the Al-5Nb-1B alloy treated with 1000 W ultrasonic power is presented. From the back-scattered map shown in Fig. 5a, it can be observed that

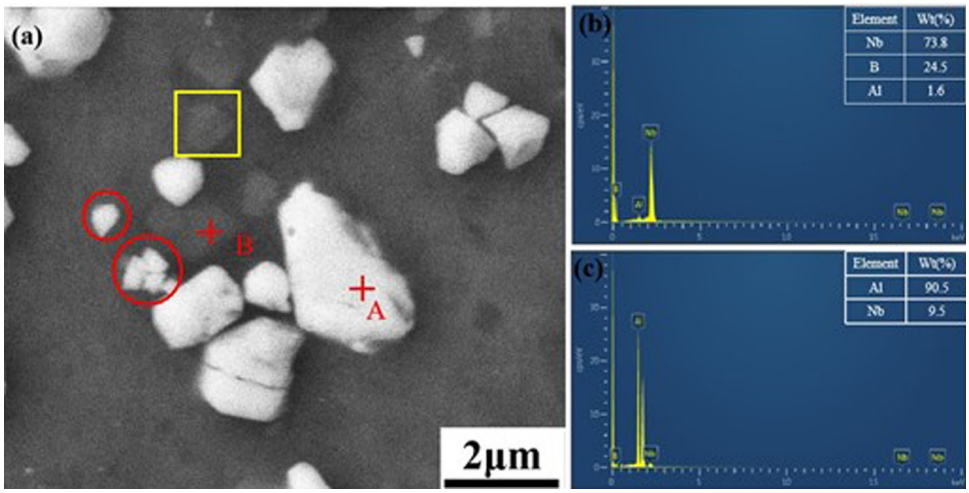

Fig. 4 EDS analysis of second phases in Al-5Nb-1B alloy with 1000 W ultrasonic power: (a) back-scattered electron image; (b) A point analysis; (c) B point analysis

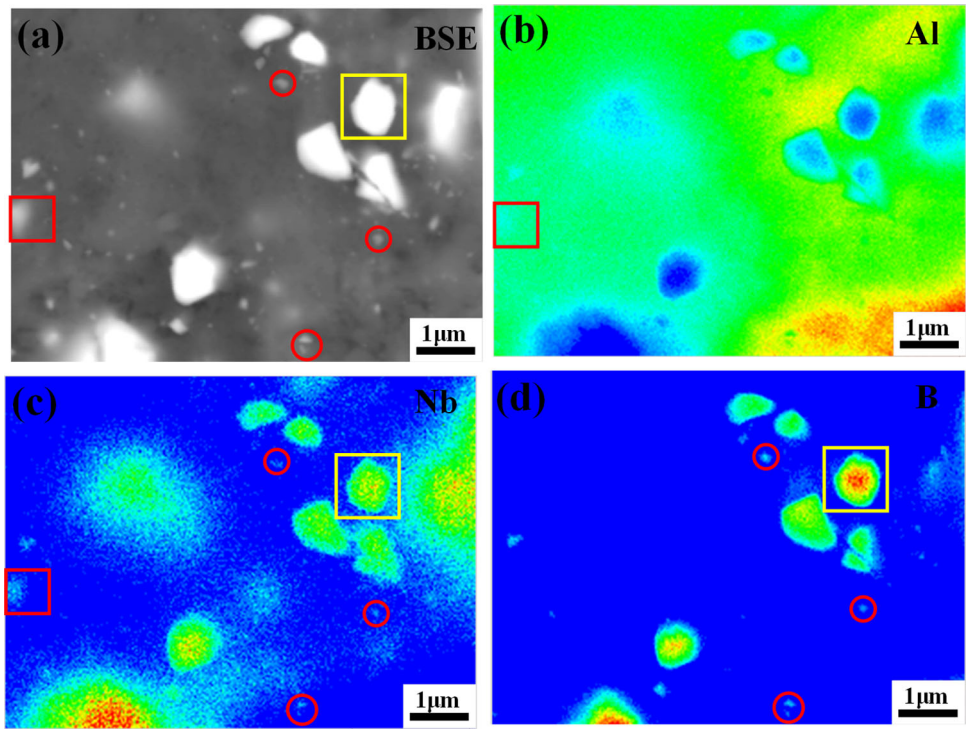

Fig. 5 EPMA mapping analysis of Al-5Nb-1B alloy prepared under 1000 W ultrasonic power condition: (a) back-scattered electron image; (b) Al element; (c) Nb element; (d) B element

there are white block phases and gray mass precipitates with a mean size of 1.3 μm distributed on the Al matrix. In addition, it can be found from the mapping analysis that the white phases (indicated by the yellow square in Fig. 5) consist of Al, Nb, and B elements. Combining the results of point analysis in Fig. 4, the Nb/B mass ratio is close to 1:2 after excluding the interference of the Al matrix. Hence, it can be inferred that white block phases should be NbB_2 particles. Furthermore, it is evident that the gray phases are composed of Al and Nb elements, as shown in Fig. 5b and c. It has been presented in previous literature (Ref 22) that the Al_3Nb particles can be formed in addition to the precipitating fine NbB_2 particles in the Al-5Nb-1B alloy in solidification. Therefore, combining XRD and mapping analysis of elements (Fig. 5), it can be concluded that the gray phases marked by the red square in Fig. 5 should be Al_3Nb phases. Additionally, according to the analysis of Fig. 5, the fine white particles are formed (indicated by the red circle in Fig. 5), which can be identified as NbB_2 phases with an average size of 169 nm.

Figure 6 and 7 show the change of morphology and average size of NbB_2 and Al_3Nb particles distributed in S1, S2, S3, and S4 alloys. Figure 6(a) indicates the shape of precipitating phases in Al-5Nb-1B alloy without UT. As shown in Fig. 6(a), it is obviously observed that the NbB_2 particles with the mean

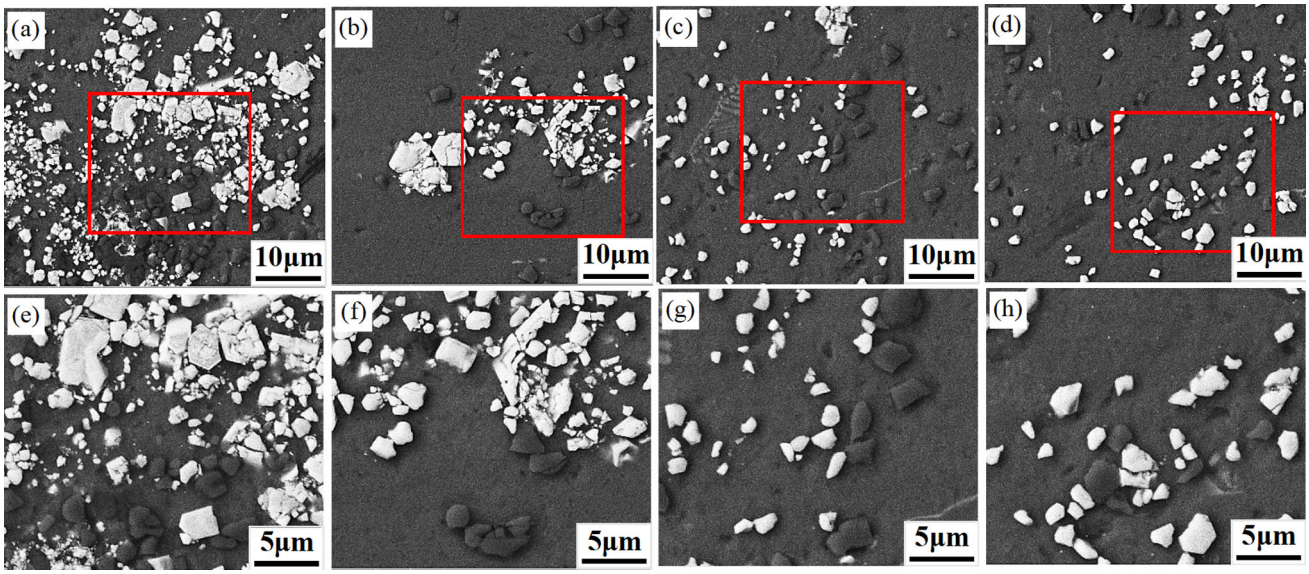

Fig. 6 Second phases in Al-5Nb-1B alloy at different ultrasonic power: (a) and (e)S1 ; (b) and (f) S2; (c) and (g) S3; (d) and (h) S4.

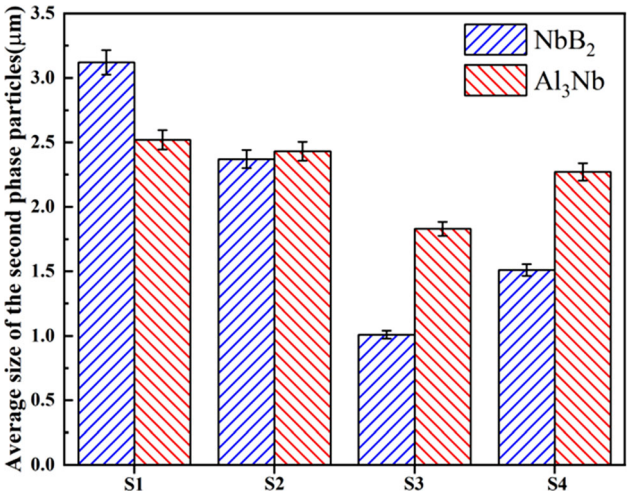

Fig. 7 Influence of ultrasonic power on the average size of NbB_2 and Al_3Nb particles in Al-5Nb-1B alloy

size of 3.12 μm agglomeratively exist in the form of coarse irregular masses and the Al_3Nb phases are inhomogeneously distributed in the Al matrix. Figure 6(b) illustrates the distribution of precipitating particles in S2 alloy. It is obviously observed that only a portion of the segregation NbB_2 particles are transformed into the block. Despite the melt treated by 500 W ultrasonic power, the morphology and size of the Al_3Nb phases are almost not changed. However, most of the NbB_2 and Al_3Nb phases in S3 sample precipitate in the form of small blocks in solidification, as shown in Fig. 6(c). Moreover, these fine particles are distributed homogeneously in the α-Al matrix. Simultaneously, comparing with S1 alloy, the size of NbB_2 and Al_3Nb phases is decreased by 208.9 and 37.7% from 3.12 and 2.52 μm to 1.01 and 1.86 μm, respectively. However, it can be clearly found from the S4 alloy that the size of some NbB_2 and Al_3Nb precipitates is not further decreased. Moreover, the coarsening phenomenon happens and the size increases to 1.51 and 2.27 μm, respectively.

3.3 Mechanism of Microstructure Refinement

Figure 8 indicates the relationship between primary α-Al phases, NbB_2 and Al_3Nb particles. The refinement mechanism of primary α-Al of Al-5Nb-1B alloy with UT of 1000 W is investigated. Figure 8a illustrates the secondary electron micrograph of the alloy, and the local magnification in the red square is inserted in the top-right corner. The micrograph displays the distribution of bright white particles (point A) in the α-Al matrix. The composition analysis of point A through EDS indicates that the fine particle is composed of Nb and B elements, as shown in Fig. 8(a) and (b). The result indicates that the bright white particles should be NbB_2 precipitates. Previous studies have demonstrated that the (10-11) plane of NbB_2 can act as heterogeneous nucleation sites refining primary α-Al (Ref 23). Additionally, the elemental mapping distribution reveals that the Nb content on the surface of NbB_2 particles decreases and Al content increases, suggesting that the Al-enriched layer is formed on the particle surface, as shown in Fig. 5. It is reported that some Nb atoms can be replaced by Al atoms in NbB_2 precipitates, leading to the (Al, Nb)B_2 intermediate layer formation. The unique intermediate layer is believed to enhance the heterogeneous nucleation ability of NbB_2 (Ref 24, 25). Furthermore, Xu et al. (Ref 15) investigated the microstructure evolution and grain refinement capacity of Al-xNb-yB alloy under different Nb/B ratios and found that the orientation relationship between $NbAl_3$ and α-Al is identified: $(001)_{Al3Nb}//(010)_{\alpha\text{-}Al}$. The α-Al phase shows a face-centered cubic (FCC) structure having the lattice parameter of a = 0.405 nm. In contrast, Al_3Nb has a tetragonal structure, with lattice parameters a = 0.3844 nm and c = 0.8609 nm. The calculated lattice misfit between Al_3Nb and α-Al is about 4.5%. When the lattice mismatch is less than 8 %, the substrate is referred to as a potential nucleation sites (Ref 26. Thus, Al_3Nb particles can also act as effective nuclei of the α-Al phase during the process of Al alloy solidification.

As shown in Fig. 9, DSC analysis is performed on S1 and S3 alloys to study the effect of ultrasonic treatment on the temperature of solidus and liquidus of the primary α-Al phase. The data reveal a significant increase in T_a, and the actual

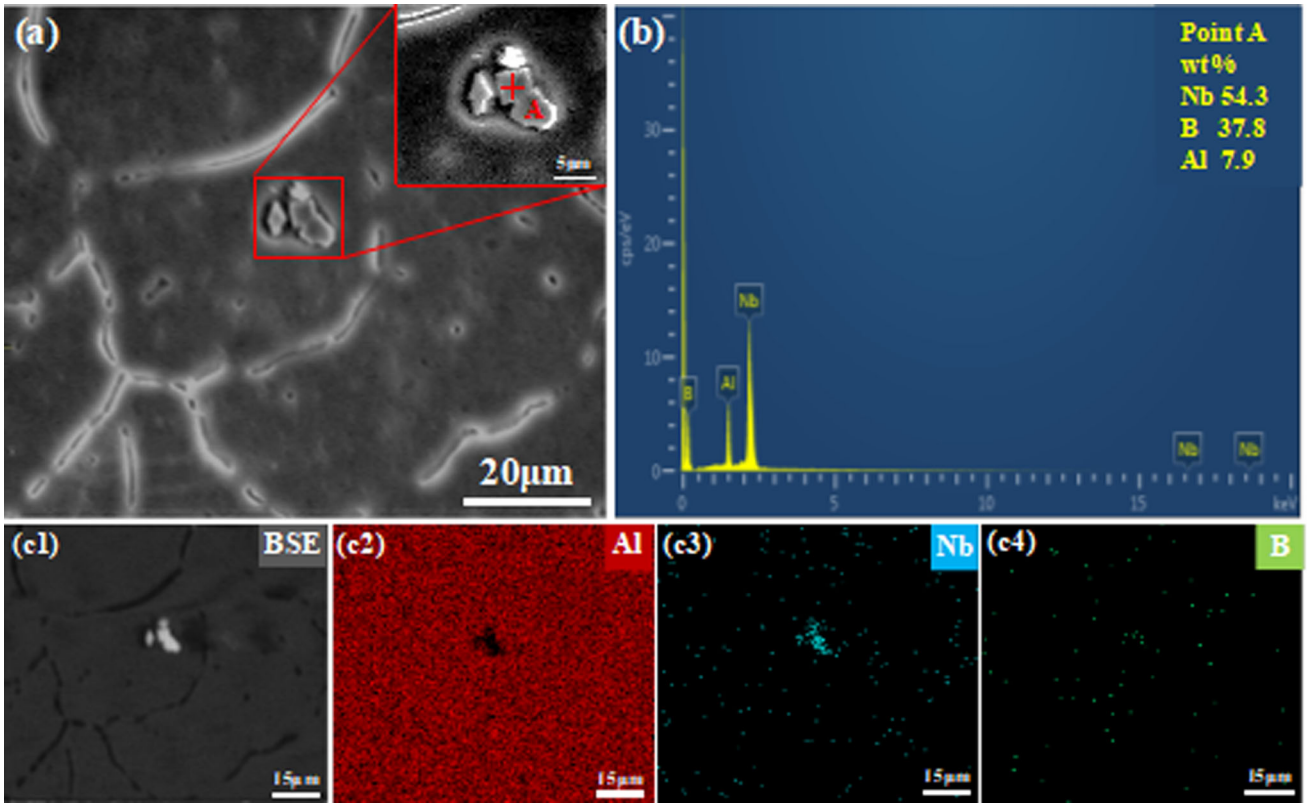

Fig. 8 SEM images of Al-5Nb-1B alloy after 1000 W ultrasonic treatment: (a) Typical NbB_2 nucleation core in the center of α-Al grains (the red square on the right is a partial magnification of the image); (b) EDS analysis and elemental composition at point A; (c1-c4) EDS mapping of Al, Nb, and B elements

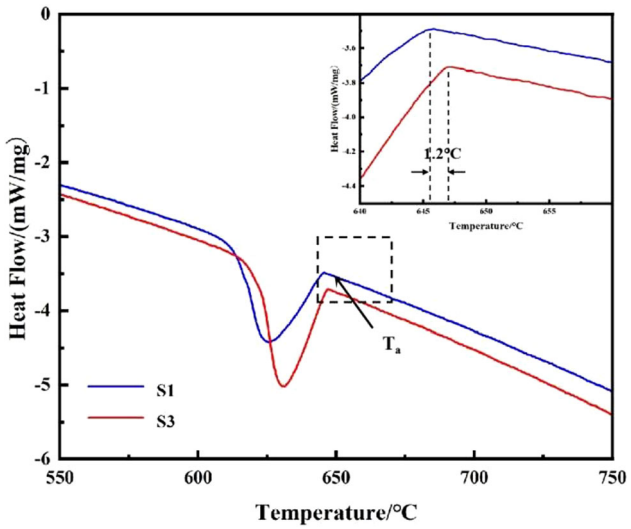

Fig. 9 DSC curves of S1 and S3 alloys

solidification temperature of the α-Al phase is increased from 650.3 to 652.9 °C after UT of 1000 W. The DSC analysis indicates that the real solidification temperature of the α-Al phase is raised by 1.7 °C after UT. It has been reported that the actual nucleation temperature of the Al-10Cu alloy after UT was reduced by 4 °C compared with the conventional solidification, which was attributed to the enhancement of heterogeneous nuclei due to acoustic cavitation (Ref 27). Hence, the nucleation supercooling of the α-Al phase reduces when the alloy melt is treated by the application of ultrasonic vibration and α-Al phase of Al-5Nb-1B alloy is effectively refined.

In addition, it can be shown in Fig. 8 that the distribution and size of NbB_2 and Al_3Nb particles in Al-5Nb-1B alloy are significantly optimized by the melt ultrasonic treatment, which should be attributed to producing nonlinear effects including acoustic cavitation (Ref 28, 29) and streaming (Ref 30). When the alloy melt is treated by ultrasonic vibration, small cavitation bubbles can be formed in the liquid due to the tensile stress of ultrasound. Under sufficiently high sound pressure, some cavitation bubbles continue to grow and then collapse and breakdown rapidly, resulting in the formation of local high-temperature and high-pressure regions in the liquid. Suslik et al. (Ref 31) presented that the local temperature and pressure reached 5000 K and 1000 atm during the collapse of cavitation bubbles. When the sound intensity (P_k) is higher than 1×10^6 Pa, cavitation sound waves occur in light material (Ref 32). According to previous investigation (Ref 33), the sound intensity P_k can be determined using the following equation:

$$P_k = \left(\frac{2P\rho_L c_L}{A}\right)^{1/2}$$

where P_k is the ultrasonic input power in watts, ρ_L is the melt density in kg/m^3, c_L is the propagation velocity of ultrasound in the melt in m/s, and A is the cross-sectional area of the ultrasonic probe in m^2. In this study, the input power is 500, 1000, and 1500 W, respectively. The Al-5Nb-1B melt density is

2.37×10^3 kg/m^3 (Ref 33), c_L is 4.6×10^3 m/s (Ref 34), and A is 4.52 cm^2. According to these parameters, it is obtained that P_k is 2.37×10^6, 6.95×10^6, and 8.51×10^6 Pa, respectively, which is higher than the minimum threshold value required for acoustic cavitation (1×10^6 Pa) (Ref 35). Therefore, the implosion of cavitation bubbles can take place during UT.

Figure 10 is a schematic diagram of optimizing the distribution and decreasing the size of NbB_2 and Al_3Nb particles in Al-5Nb-1B alloy through the cavitation and acoustic streaming effect. A large number of cavitation bubbles is first generated in the melt during the ultrasonic vibration, and the cavitation bubbles undergo growth, rapid expansion, and finally collapse and breakdown. During the melt ultrasonic treatment, cavitation bubbles also can increase the heterogeneous nucleation ability and refine the grains. On the one hand, when cavitation bubbles grow rapidly, liquid evaporates inside the bubbles. The evaporation of liquids and expansion of bubbles tend to decrease the temperature of the bubbles. When the bubble temperature is lower than the equilibrium melting point, it will lead to an undercooling of the melt at the bubble and the number of nucleations on the bubbles increases (Ref 36). Therefore, ultrasonic melt treatment not only effectively refines α-Al, but also optimizes the size and distribution of the second phases. On the other hand, when the cavitation bubble collapses, a large number of pressure pulses will be generated. At the same time, a transient high-pressure shock wave also generates and the large blocky NbB_2 is refined into a fine particles, and homogeneously distributes in the primary α-Al matrix (Ref 37). In addition, the whirlpools that are generated by acoustic streaming significantly enhance the chance of collision on Al_3Nb and NbB_2 particles in the melt. Thus, the segregation of Al_3Nb and NbB_2 particles is weakened. Meanwhile, under acoustic streaming, the broken Al_3Nb and NbB_2 particles are homogeneously dispersed in the melt. Specifically, the cavitation bubbles do not grow completely, which breaks up agglomeration of the precipitating phase after ultrasonic melt treatment of 500 W power, as shown in Fig. 6(b). When the alloy melt is treated by 1000 W ultrasound power, the majority of the NbB_2 and Al_3Nb phases are transformed into small blocks. Nevertheless, as the ultrasound power is further improved to 1500 W, the Al_3Nb and NbB_2 particles occur to the coarsening. It has been reported in the literature (Ref 38) that when the ultrasound power is increased to a certain value, a large amount of energy is introduced and converted into heat in alloy melt, which causes the cooling rate to decline and weakens the influence of UT on grain refinement.

3.4 The Refinement of Al-7Si Alloy

Figure 11 and 12 show the optical microstructure of α-Al phase and the change of SDAS of Al-7Si alloy by adding S1, S2, S3, and S4 alloys. It is found that the unrefined Al-7Si alloy illustrates a typical coarse dendrite and the SDAS is approx-

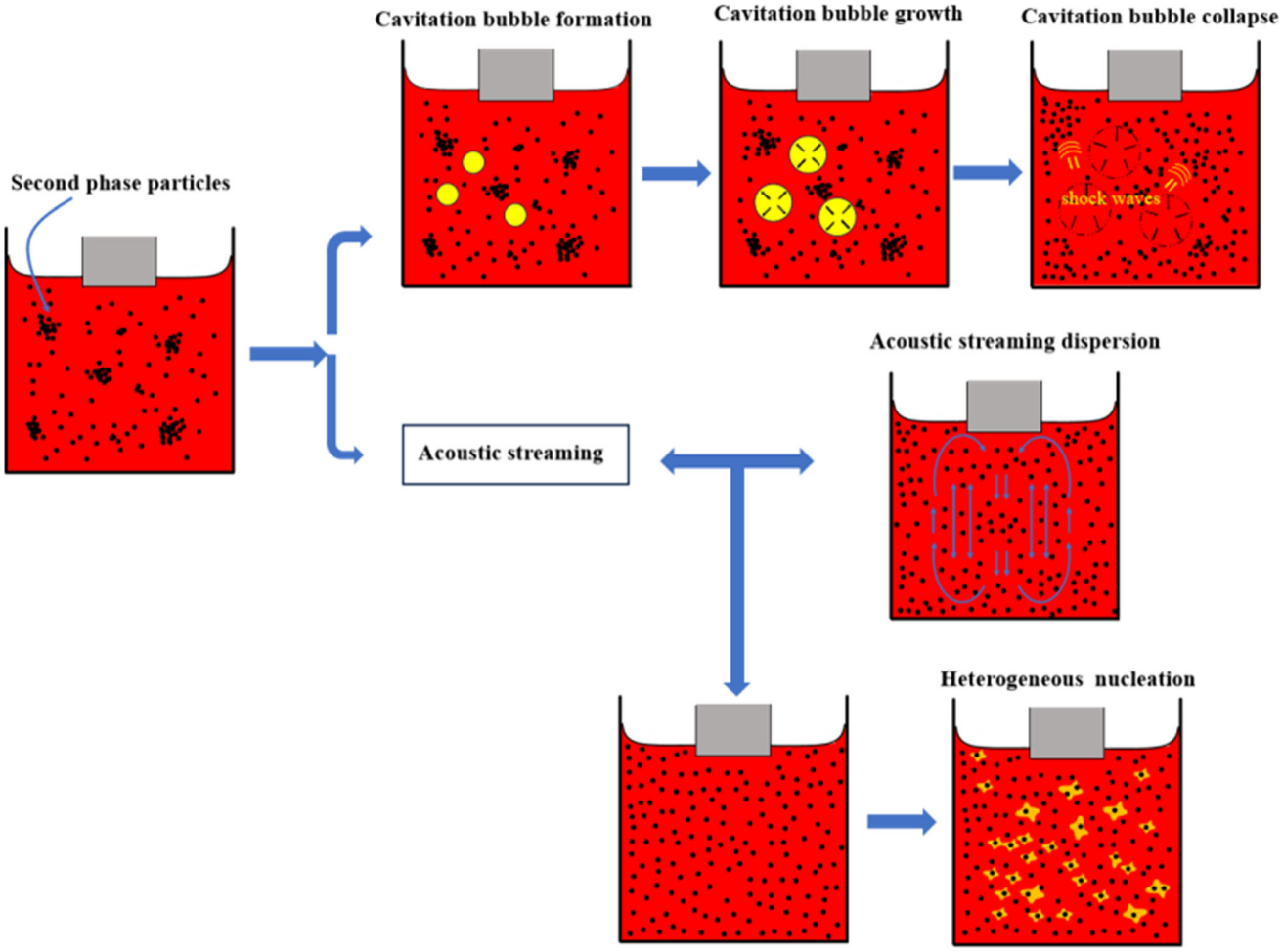

Fig. 10 Schematic diagram of acoustic cavitation and acoustic streaming effect in the Al-5Nb-1B melt

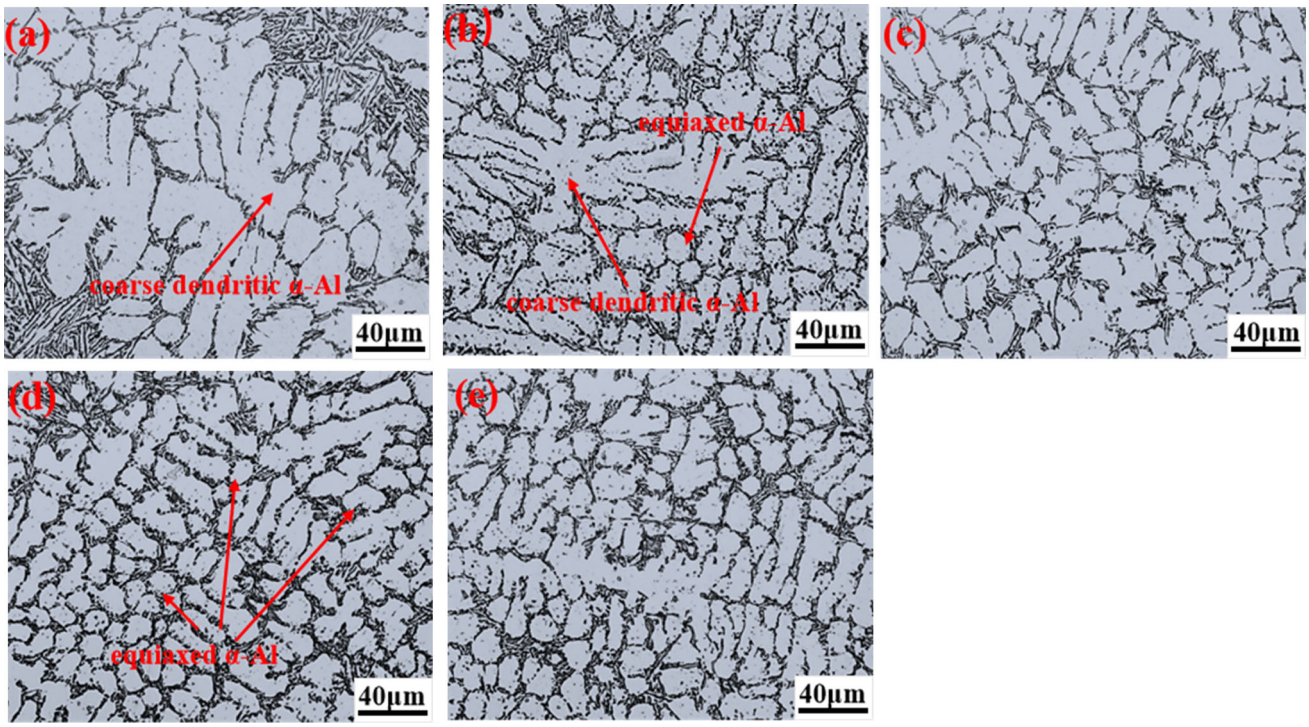

Fig. 11 The effect of Al-5Nb-1B master alloy on α-Al phase:(a) unrefined Al-7Si alloy; (b) Al-7Si + S1 alloy; (c) Al-7Si + S2 alloy; (d) Al-7Si + S3 alloy; (e) Al-7Si + S4 alloy

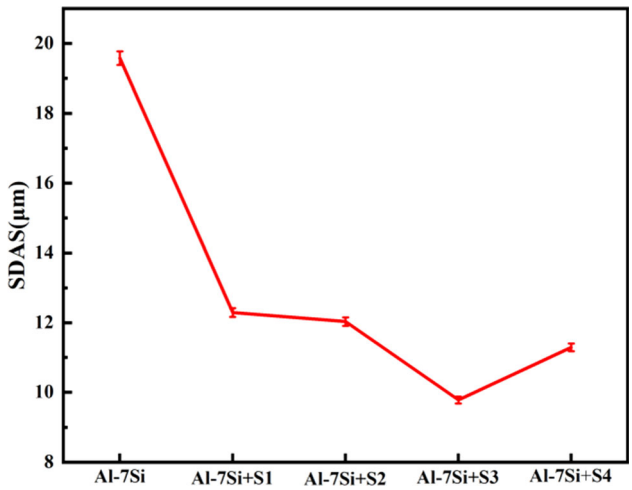

Fig. 12 SDAS of α-Al in Al-7Si alloy with Al-5Nb-1B master alloy treated by the different power

imately 19.58 μm, as shown in Fig. 11(a). With the addition of Al-5Nb-1B alloy, it can be observed that the morphology and the grains size of α-Al phase occur to substantial change. In Fig. 11(b), when S1 alloy is introduced into the Al-7Si alloy, a part of the α-Al dendrites is refined into equiaxed crystals resulting in a reduction of the SDAS to 12.29 μm. After introducing S2 alloy to Al-7Si alloy, the microstructure and grain size of the α-Al phase do not happen to significantly change. Simultaneously, the SDAS also is the same as the Al-7Si alloy with S1 alloy addition. Upon introducing S3 alloy, the α-Al phase of Al-7Si alloy is greatly refined from coarse dendrites to fine equiaxed grains, as illustrated in Fig. 11(d). Compared with unrefined Al-7Si alloy, the SDAS is obviously decreased by 100.2% from 19.58 to 9.78 μm. However, it is found from Fig. 11(e) that when S4 alloy is added, the α-Al occurs to coarsening and the SDAS increases to 11.29 μm. In summary, the refinement effect of α-Al phase in Al-7Si alloy with the addition of S3 alloy is best, and the fine equiaxed crystals can be obtained.

The refinement impact is related to the size and shape of the second phases, as well as the distributing state in master alloys acting as refiners (Ref 7, 39, 40). If the second phases happen to agglomeration, it is difficult to disperse nucleation particles when the refiners are added to aluminum alloys melting due to hereditary effect and diminishes the refining ability (Ref 41). It is known that NbB_2 and Al_3Nb particles can serve as heterogeneous nucleation sites for α-Al in Al alloys. At the same time, the application of UT effectively changes the size and distribution of NbB_2 and Al_3Nb particles in the Al-5Nb-1B master alloy. When the ultrasonic power is 1000 W, the Al_3Nb and NbB_2 particles in the Al-5Nb-1B alloy are evenly distributed on the Al matrix, and the size of Al_3Nb and NbB_2 particles is also the smallest. Therefore, the grains refinement effect of Al-7Si alloy refiner is the most outstanding when the Al-5Nb-1B master alloy treated by 1000 W ultrasonic power is added.

Figure 13(a) shows the stress–strain curves of Al-7Si alloy with adding S1, S2, S3, and S4 alloys. Figure 13(b) shows the changes of UTS and El of the Al-7Si alloy before and after refinement. The addition of Al-5Nb-1B master alloy is found to effectively enhance the mechanical properties of Al-7Si alloy. The introduction of S1 alloy as a refiner shows that the UTS is increased from 171 to 180.3 MPa, and the El is also enhanced from 7.1 to 10.8%. When S2 alloy is added, the mechanical properties of the Al-7Si alloy do not change significantly. After adding S3 alloy to Al-7Si alloy, the mechanical properties significantly improved. The UTS is improved by 10.2% from

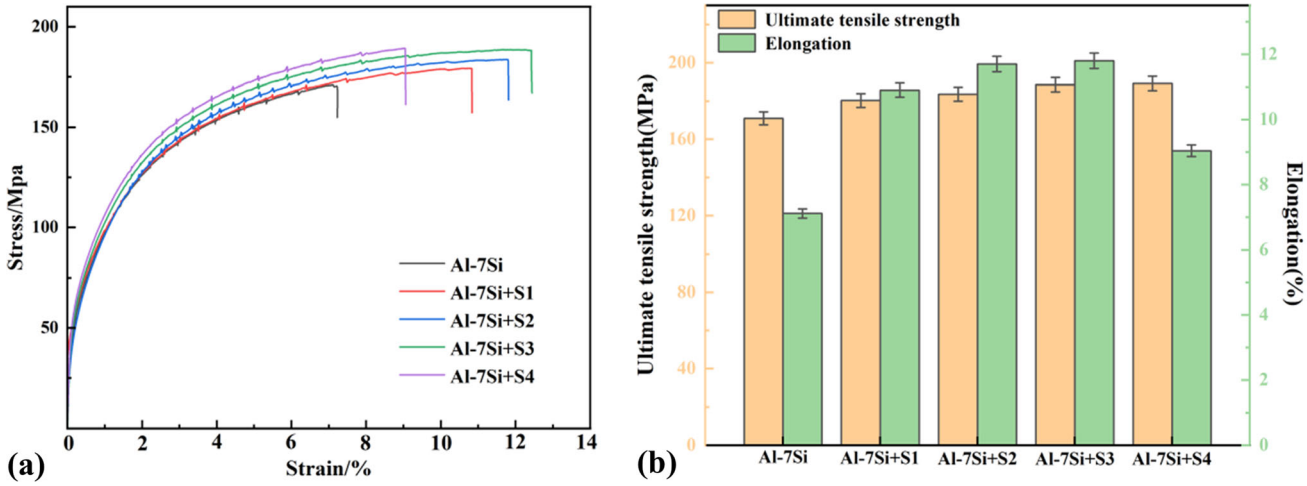

Fig. 13 Mechanical properties of Al-7Si alloy with Al-5Nb-1B master alloy addition

171 to 188.5 MPa, and the El is enhanced by 66.2% from 7.1 to 11.8%. However, the UTS and El begin to decrease after the addition of S4 alloy. It is consistent with the primary α-Al evolution of Al-7Si alloy after refiner treated by the different ultrasonic power. In accordance with the Hall–Petch formula (Ref 42):

$$\sigma_s = \sigma_0 + kd^{-1/2}$$

where, σ_s reflects the strength of the alloy, σ_0 represents the strength of a single crystal, k is a constant related to the material, and d is the average grain size. Based on the formula, it is evident that the strength of the alloys is increased with the decrease in grain size. This is because the resistance to dislocation movement during plastic deformation increases as the number of grain boundaries increases, and the development of microcracks merging and cracks propagation is inhibited, which significantly improves the mechanical properties of Al-7Si alloy.

Figure 14 reveals the tensile fracture surface of Al-7Si alloy with adding Al-5Nb-1B master alloy treated by different ultrasonic power. Figure 14(a), (b), and (c) is the fracture morphology of the unrefined Al-7Si alloy. The fracture surface is observed to consist of multiple cleavage planes, which is a typical brittle fracture. In comparison, the microstructure of the Al-7Si alloy was significantly refined with the introducing S1 and S2 alloy. The size of the cleavage planes on the fracture surface decreases, and a small number of dimples begin to appear. The fracture mode changes from brittle fracture to ductile–brittle mixture fracture, as shown in Figure 14(d), (e), and (f). When S3 alloy is added, it can be found from Fig j-l that the fracture surface of Al-7Si alloy is basically large and deep dimples, which are very obvious ductile fracture features. After the introduction of S4 alloy, the dimples on the alloy fracture surface occur to reduce, and the fine cleavage planes appear, which is in agreement with the α-Al coarsening of the Al-7Si alloy

4. Conclusions

The grain refinement and mechanical properties of Al-7Si alloy with Al-5Nb-1B master alloy addition treated by ultrasound treatment were studied and the key conclusions were as follows:

(1) When ultrasonic power of 1500 W was applied in Al-5Nb-1B alloy melt, α-Al was obviously refined from the coarse cellular morphology into the small equiaxed structure, and the grain sizes were decreased by 109.7% from 125 to 60 μm.
(2) The NbB_2 and Al_3Nb particles of Al-5Nb-1B alloy can be significantly refined into fine blocks after the melting is ultrasound treated, and the agglomerated phenomenon of NbB_2 particles disappears. Moreover, the size of NbB_2 and Al_3Nb particles in Al-5Nb-1B alloy treated by 1000 W ultrasonic power was smaller than that of 500 and 1500 W.
(3) After Al-7Si alloy is treated with ultrasonic prepared Al-5Nb-1B master alloy, the α-Al phase is significantly refined from the coarse dendrites to fine equiaxed crystals.

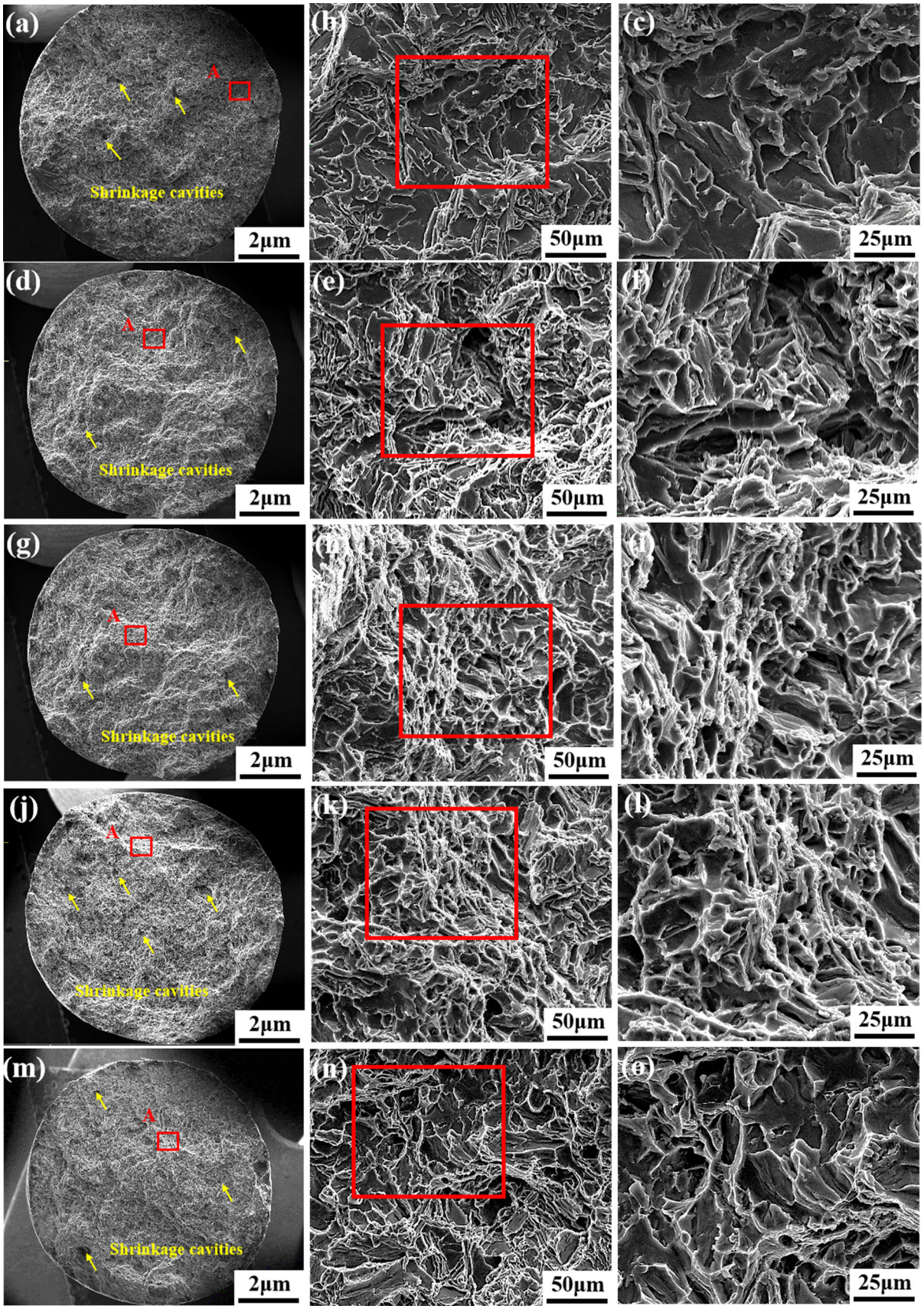

Fig. 14 Fracture surface morphology of Al-7Si alloy with Al-5Nb-1B master alloy: (a-c) unrefined Al-7Si alloy; (d-f) Al-7Si + S1 alloy; (g-i) Al-7Si + S2 alloy; (j-l) Al-7Si + S3 alloy; (m-o) Al-7Si + S4 alloy

(4) The mechanical properties of Al-7Si alloy are also significantly improved. When the Al-5Nb-1B master alloy treated by 1000 W ultrasonic power was added to Al-7Si alloy as a refiner, the UTS of the alloy was improved by 10.2% from 171 to 188.5 MPa, and the El was enhanced by 66.2% from 7.1 to 11.8%. Moreover, the fracture mode of the alloy happens to change from brittle to ductile.

Acknowledgments

The authors are indebted to the National Natural Science Foundation of China (Grant No. 52061026; No. 51561021), Key R&D Program of Gansu Province (21YF5GA075), the Natural Science Foundation of Gansu Province (23JRRA752; 22JR5-RA251; 21JR7RA216), and Gansu Province Outstanding Graduate Student "Innovation Star" Project (2023CXZX392) for their support.

References

1. Z. Fan, Y. Wang, Y. Zhang, T. Qin, X.R. Zhou, G.E. Thompson, T. Pennycook, and T. Hashimoto, Grain Refining Mechanism in the Al/Al-Ti-B System, *Acta Mater.*, 2015, **84**, p 292–304
2. Q. Zheng, Z. Ye, H. Jiang, M. Lu, L. Zhang, and J. Zhao, Effect of Micro-Alloying Element La on Solidification Microstructure and Mechanical Properties of Hypoeutectic Al-Si Alloys, *Acta Metall. Sin.*, 2017, **57**(1), p 103–110
3. H. Jiang, Q. Sun, L. Zhang, and J. Zhao, Al-Ti-C Master Alloy with Nano-Sized TiC Particles Dispersed in the Matrix Prepared by Using Carbon Nanotubes as C Source, *J. Alloy. Compd.*, 2018, **748**, p 774–782
4. H. Jiang, Y. Song, L. Zhang, J. He, S. Li, and J. Zhao, Efficient Grain Refinement of Al Alloys Induced by in-situ Nanoparticles, *J. Mater. Sci. Technol.*, 2022, **124**, p 14–25
5. Y. Li, B. Hu, B. Liu, A. Nie, Q. Gu, J. Wang, and Q. Li, Insight into Si Poisoning on Grain Refinement of Al-Si/Al-5Ti-B System, *Acta Mater.*, 2020, **187**, p 51–65
6. T.E. Quested, A.T. Dinsdale, and A.L. Greer, Thermodynamic Evidence for a Poisoning Mechanism in the Al-Si-Ti System, *Mater. Sci. Technol.*, 2013, **22**(9), p 1126–1134
7. Z. Fan, F. Gao, Y. Wang, H. Men, and L. Zhou, Effect of Solutes on Grain Refinement, *Prog. Mater. Sci.*, 2022, **123**, p 100809
8. Y. Birol, AlB_3 Master Alloy to Grain Refine AlSi10Mg and AlSi12Cu Aluminum Foundry Alloys, *J. Alloy. Compd.*, 2012, **513**, p 150–153
9. P. Li, S. Liu, L. Zhang, and X. Liu, Grain Refinement of A356 Alloy by Al-Ti-B-C Master Alloy and its Effect on Mechanical Properties, *Mater. Des.*, 2013, **47**, p 522–528
10. M. Nowak, L. Bolzoni, and N. Hari Babu, Grain Refinement of Al-Si Alloys by Nb-B Inoculation. Part I: Concept Development and Effect on Binary Alloys, *Mater. Des.*, 2015, **66**, p 366–375
11. Z. Li, C. Liao, Y. Liu, X. Wang, Y. Wu, M. Zhao, Z. Long, and F. Yin, 700 °C Isothermal Section of the Al-Ti-Si Ternary Phase Diagram, *J. Phase Equilib. Diffus.*, 2014, **35**(5), p 564–574
12. T. Gao, P. Li, Y. Li, and X. Liu, Influence of Si and Ti Contents on the Microstructure, Microhardness and Performance of TiAlSi Intermetallics in Al-Si-Ti Alloys, *J. Alloy. Compd.*, 2011, **509**(31), p 8013–8017
13. L. Bolzoni, M. Nowak, and N. Hari Babu, Assessment of the Influence of Al-2Nb-2B Master Alloy on the Grain Refinement and Properties of LM6 (A413) Alloy, *Mater. Sci. Eng. A*, 2015, **628**, p 230–237
14. L. Bolzoni and N.H. Babu, Refinement of the Grain Size of the LM25 Alloy (A356) by 96Al-2Nb-2B Master Alloy, *J. Mater. Process. Technol.*, 2015, **222**, p 219–223
15. J. Xu, Y. Li, B. Hu, Y. Jiang, and Q. Li, Development of Al-Nb-B Master Alloy with High Nb/B Ratio for Grain Refinement of Hypoeutectic Al-Si Cast Alloys, *J. Mater. Sci.*, 2019, **54**(23), p 14561–14576
16. J. Li, F. Li, S. Wu, S. Lü, W. Guo, and X. Yang, Variation of Microstructure and Mechanical Properties of Hybrid Particulates Reinforced Al-alloy Matrix Composites with Ultrasonic Treatment, *J. Alloy. Compd.*, 2019, **789**, p 630–638
17. R.K. Gupta, J. Nampoothiri, S. Dhamodharan, K.R. Ravi, V. Udhayabanu, and D.R. Peshwe, Ultrasonic Assisted Synthesis of Al-Cu/2 vol%Grp Composite and its Characterization, *J. Alloy. Compd.*, 2020, **845**, p 156087
18. J.G. Jung, S.H. Lee, J.M. Lee, Y.H. Cho, S.H. Kim, and W.H. Yoon, Improved Mechanical Properties of Near-eutectic Al-Si Piston Alloy Through Ultrasonic Melt Treatment, *Mater. Sci. Eng. A*, 2016, **669**, p 187–195
19. Z. Liu, P. Xie, M. Chen, Q. Zheng, Y. Gao, Y. Liu, and X. Kai, Effects of Ultrasound Assisted Solidification on the Microstructure and Mechanical Properties of Nano-Sized TiB_2/Al-45Cu Composites, *Materialia*, 2021, **15**, p 101024
20. Y. Han, K. Li, J. Wang, D. Shu, and B. Sun, Influence of High-Intensity Ultrasound on Grain Refining Performance of Al-5Ti-1B Master Alloy on Aluminum, *Mater. Sci. Eng. A*, 2005, **405**(1–2), p 306–312
21. G. Wu, X. Tong, R. Jiang, and W. Ding, Grain Refinement of as-cast Mg-RE Alloys: Research Progress and Future Prospect, *Acta Metall. Sin.*, 2022, **58**(4), p 385–399
22. S. Jha, A. Mandal, and P. Srirangam, Optimization of Casting Process Parameters for Synthesis of Al-Nb-B Master Alloy, *Jom*, 2018, **71**(1), p 397–406
23. J. Ding, C. Cui, Y. Sun, J. Shi, S. Cui, and Q. Ma, Preparation of in Situ Al_3Nb-NbB_2-NbC/Al Inoculant and its Effect on Microstructures and Properties of Weldable Al-Cu-Mn Alloy, *Mater. Sci. Eng. A*, 2018, **738**, p 273–282
24. Y. Li, Y. Jiang, B. Hu, and Q. Li, Novel Al-Ti-Nb-B Grain Refiners with Superior Efficiency for Al-Si Alloys, *Scripta Mater.*, 2020, **187**, p 262–267
25. Y. Li, Y. Jiang, B. Liu, Q. Luo, B. Hu, and Q. Li, Understanding Grain Refining and Anti Si-poisoning Effect in Al-10Si/Al-5Nb-B System, *J. Mater. Sci. Technol.*, 2021, **65**, p 190–201
26. J. Liu, L. Zhang, and G. Ge, Study of the Orientation Relationship of the Residual α2(Ti_3Al) in γ(TiAl) Sheet After Heat Treatment, *J. Mater. Eng. Perform.*, 2022, **31**(5), p 4224–4231
27. H.R. Kotadia, M. Qian, D.G. Eskin, and A. Das, On the Microstructural Refinement in Commercial Purity Al and Al-10wt%Cu Alloy Under Ultrasonication During Solidification, *Mater. Des.*, 2017, **132**, p 266–274
28. R. Gupta and B.S.S. Daniel, Strengthening Mechanisms in Al_3Zr-Reinforced Aluminum Composite Prepared by Ultrasonic Assisted Casting, *J. Mater. Eng. Perform.*, 2021, **30**(4), p 2504–2513
29. R. Haghayeghi, L.C. de Paula, and E.J. Zoqui, Comparison of Si Refinement Efficiency of Electromagnetic Stirring and Ultrasonic Treatment for a Hypereutectic Al-Si Alloy, *J. Mater. Eng. Perform.*, 2017, **26**(4), p 1900–1907
30. Q. Cui, L. Ma, C. Zhu, C. Zhou, Y. Song, and J. Liang, Grain Refinement and Mechanical Property Improvements in Ultrasound-Assisted Brazing of SiCp/Al Composite Materials, *J. Mater. Eng. Perform.*, 2022, **31**(6), p 4974–4982
31. K.S. Suslick, J.R. BlakePerutz, Y. Didenko, M.M. Fang, T. Hyeon, K.J. Kolbeck, W.B. McNamara, M.M. Mdleleni, and M. Wong, Acoustic Cavitation and its Chemical Consequences, *Philos. Trans. Royal Soc. London Series A: Math. Phys. Eng. Sci.*, 1999, **357**(1751), p 335–353
32. S.V. Sujith, H. Kim, R.S. Mulik, H. Park, and J. Lee, Synergistic Effect of in-situ Al-7075/Al_3Ti Metal Matrix Composites Prepared Via Stir-Assisted Ultrasonic Melt Processing Under Dynamic Nucleation, *Met. Mater. Int.*, 2022, **28**(9), p 2288–2303
33. P. Pragathi and R. Elansezhian, Mechanical and Microstructure Behaviour of Aluminum Nanocomposite Fabricated by Squeeze Casting and Ultrasonic Aided Squeeze Casting: A Comparative Study, *J. Alloy. Compd.*, 2023, **956**, p 17203
34. J. Xu, R. Li, and Q. Li, Effect of Agglomeration on Nucleation Potency of Inoculant Particles in the Al-Nb-B Master Alloy: Modeling and Experiments, *Metall. Mater. Trans. A*, 2021, **52**(3), p 1077–1094
35. Z. Liu, P. Xie, M. Chen, Q. Zheng, Y. Gao, Y. Liu, and X. Kai, Effects of Ultrasound Assisted Solidificaiton on the Microstructure and Mechanical Properties of Nano-Sized TiB_2/Al-$_{4.5}$Cu Composites, *Materialia*, 2021, **15**, p 101024
36. A. Pola, L. Montesano, M. Tocci, and G. La Vecchia, Influence of Ultrasound Treatment on Cavitation Erosion Resistance of AlSi7 Alloy, *Materials*, 2017, **10**(3), p 256

37. M. Qian, A. Ramirez, and A. Das, Ultrasonic Refinement of Magnesium by Cavitation: Clarifying the Role of Wall Crystals, *J. Cryst. Growth*, 2009, **311**(14), p 3708–3715
38. Z. Shao, Q. Le, Z. Zhang, and J. Cui, Effect of Ultrasonic Power on Grain Refinement and Purification Processing of AZ80 Alloy by Ultrasonic Treatment, *Met. Mater. Int.*, 2012, **18**(2), p 209–215
39. G.S. Vinod Kumar, B.S. Murty, and M. Chakraborty, Settling Behaviour of $TiAl_3$, TiB_2, TiC and AlB_2 Particles in Liquid Al During Grain Refinement, *Int. J. Cast Metals Res.*, 2013, **23**(4), p 193–204
40. F. Gazanion, X.G. Chen, and C. Dupuis, Studies on the Sedimentation and Agglomeration Behavior of Al-Ti-B and Al-Ti-C Grain Refiners, *Mater. Sci. Forum*, 2002, **396–402**, p 45–52
41. E.B. Moustafa, M.A. Alazwari, W.S. Abushanab, E.I. Ghandourah, A.O. Mosleh, H.M. Ahmed, and M.A. Taha, Influence of Friction Stir Process on the Physical Microstructural, Corrosive, and Electrical Properties of an Al-Mg Alloy Modified with Ti-B Additives, *Materials*, 2022, **15**(3), p 835
42. J. Zhang, S.B. Kang, H. Yu, J.H. Cho, G. Min, and V.Y. Stetsenko, Effect of Fine-Grained Raw Material Addition on Microstructure Refinement and Tensile Properties in Horizontal Continuous Casting Al-12%Si Alloy Billets [J], *Mater. Design*, 2011, **32**(6), p 3566–3569